

# Dilepton emission rates from hot hadronic matter

Thorsten Renk\*

*Physik Department, Technische Universität München, D - 85745, Garching, Germany*

Amruta Mishra†

*Institut für Theoretische Physik, Robert Mayer Str. 8-10,  
D-60054 Frankfurt am Main, Germany*

(Dated: March 30, 2022)

## Abstract

The vacuum polarisation effects from the nucleon sector lead to large medium modifications of the vector meson masses in the Walecka model. With a quantum hadrodynamic framework including the quantum effects, and using a quasiparticle description for quark gluon plasma (QGP), the dilepton emission rate from the hot and dense matter resulting from relativistic nuclear collisions is calculated. Using a model for the fireball evolution which has been shown to reproduce other observables such as charmonium suppression, photon emission and the abundance of hadronic species, we compare with the dilepton invariant mass spectrum measured by the CERES collaboration at CERN SPS. We also compare the results to a previous calculation where the spectral function of a virtual photon (a key ingredient for the emission rate) has been calculated in a chiral SU(3) model.

---

\*Electronic address: [trenk@physik.tu-muenchen.de](mailto:trenk@physik.tu-muenchen.de)

†Electronic address: [mishra@th.physik.uni-frankfurt.de](mailto:mishra@th.physik.uni-frankfurt.de)

## 1. INTRODUCTION

The study of the in-medium properties of the vector mesons ( $\rho$  and  $\omega$ ) in hot and dense matter is actively investigated, both experimentally [1, 2] and theoretically [3, 4]. The experimental observation of enhanced dilepton production [1] in the low invariant mass regime possibly is due to a reduction in the vector meson masses in the medium. It was first suggested by Brown and Rho that the vector meson masses drop in the medium according to a simple scaling law [3]. Within the framework of Quantum Hadrodynamics (QHD), the vacuum polarisation effects from the baryon sector [5, 6, 7, 8] lead to a significant drop of the vector meson masses in the medium whereas the mass modification is marginal with only Fermi sea polarisation effects. The properties of the hadrons as modified in the thermal bath are reflected in the dilepton and photon spectra emitted from a hot and dense matter [8, 9, 10, 11]. Dileptons are interesting probes for the study of the hot and dense matter formed in relativistic heavy ion collisions. Since they do not interact strongly, the dileptons escape unthermalized from the hot and dense matter at all stages of the evolution. The observed enhancement of dileptons in the low invariant mass regime has initiated extensive theoretical investigations on the temperature [12] and density [13] modifications of the dileptons from hot hadronic matter as well as from a quark gluon plasma (QGP) formed in heavy ion collisions. The increased dilepton yield in S+Au collisions as observed by the CERES collaboration was attributed to enhanced  $\rho$ -meson production via  $\pi^+\pi^-$  annihilation and a dropping of the  $\rho$ -mass in the medium [14, 15]. A large broadening of the  $\rho$ -meson spectral function arising due to scattering off by baryons [16, 17] has been shown to reproduce the CERES data quite well. In the present investigation, the space-time evolution of the strongly compressed hadronic matter formed in a relativistic heavy ion collision is considered in a mixed scenario of QGP and hadronic matter. The QGP is described within a quasiparticle picture [19] and the hadronic matter described in a Quantum Hadrodynamics framework including quantum fluctuation effects from the baryon and scalar meson sectors [20, 21, 22]. The dilepton emission rates from the expanding fireball are then studied in a model based on local thermal equilibrium and isentropic expansion [23].

It was earlier demonstrated in a nonperturbative formalism that a realignment of the ground state with baryon-antibaryon condensates is equivalent to the relativistic Hartree approximation (RHA) [20]. The ground state for the nuclear matter was extended to include sigma condensates to take into account the quantum correction effects from the scalar meson sector [20]. Such a formalism includes multiloop effects and is self consistent [20, 24]. The methodology was then generalized to consider hot nuclear matter [25] as well as to study hyperon-rich dense matter [26] relevant for neutron stars. The effect of vacuum polarisations

on the vector meson properties [21] and on the static dilepton spectra [22] has also been recently studied. In the low invariant mass regime, the scalar meson contributions lead to considerable broadening the  $\omega$  peak in the dilepton spectra as compared to RHA, which leads to smearing and ultimate disappearance of the  $\omega$  peak at high densities [22]. The present investigation of dilepton spectra using a dynamical fireball model is compared with results obtained using other descriptions for hadronic matter [14, 17], as well as to the experimental results from CERES collaboration [1].

We organize the paper as follows. We first briefly recapitulate the nonperturbative framework used for studying the medium modification of the  $\omega$  and  $\rho$  vector meson properties including the vacuum fluctuation effects in the Walecka model, in section 2. Section 3 discusses the parametrisation of the photon self energy in the hadronic phase. The quark gluon plasma (QGP) phase is treated within a quasiparticle picture [19] as described in section 4. In section 5, we describe briefly the model considered for the dynamical evolution of the fireball. Section 6 deals with the calculation of dilepton emission from the fireball. Finally, we discuss the findings of the present investigation in section 7 and summarise in section 8.

## 2. VACUUM POLARISATION EFFECTS AND IN-MEDIUM VECTOR MESON PROPERTIES

We briefly recapitulate here the vacuum polarisation effects arising from the nucleon and scalar meson fields in hot nuclear matter in a nonperturbative variational framework [25] and their influence on the vector meson properties in the hot and dense matter. The method of thermofield dynamics (TFD) [27] is used here to study the “ground state” (the state with minimum thermodynamic potential) at finite temperature and density within the Walecka model with a quartic scalar self interaction. The temperature and density dependent baryon and sigma masses are also calculated in a self-consistent manner in the formalism. The ansatz functions involved in such an approach are determined through functional minimisation of the thermodynamic potential.

The Lagrangian density in the Walecka model is given as

$$\begin{aligned} \mathcal{L} = & \bar{\psi} (i\gamma^\mu \partial_\mu - M - g_\sigma \sigma - g_\omega \gamma^\mu \omega_\mu) \psi + \frac{1}{2} \partial^\mu \sigma \partial_\mu \sigma - \frac{1}{2} m_\sigma^2 \sigma^2 - \lambda \sigma^4 \\ & + \frac{1}{2} m_\omega^2 \omega^\mu \omega_\mu - \frac{1}{4} (\partial_\mu \omega_\nu - \partial_\nu \omega_\mu) (\partial^\mu \omega^\nu - \partial^\nu \omega^\mu). \end{aligned} \quad (1)$$

In the above,  $\psi$ ,  $\sigma$ , and  $\omega_\mu$  are the fields for the nucleon,  $\sigma$ , and  $\omega$  mesons with masses  $M$ ,  $m_\sigma$ , and  $m_\omega$  respectively. The quartic coupling term in  $\sigma$  is necessary for the sigma condensates to exist, through a vacuum realignment [20]. Our calculations thus include the quantum effects

arising from the sigma meson in addition to the mean field contribution from the the quartic self interaction of the scalar meson. We retain the quantum nature of both the nucleon and the scalar meson fields, whereas the vector  $\omega$ - meson is treated as a classical field, which in the mean field approximation is given as  $\langle\omega^\mu\rangle = \delta_{\mu 0}\omega_0$ . The reason is that without higher-order term for the  $\omega$ -meson, the quantum effects generated due to the  $\omega$ -meson through the present variational ansatz turn out to be zero. The thermodynamic quantities including the quantum effects can then be written down. The details regarding the formalism can be found in earlier references [20, 21, 25]. Extremisation of the thermodynamic potential, with respect to the meson fields  $\sigma_0$  and  $\omega_0$  yields the self-consistency conditions for  $\sigma_0$  (and hence for the effective nucleon mass,  $M^* = M + g_\sigma\sigma_0$ ), and for the vector meson field  $\omega_0$ . We might note here that the quantum effects arising from the scalar meson sector through  $\sigma$  meson condensates amount to a sum over a class of multiloop diagrams and, do not correspond to the one meson loop approximation for scalar meson quantum effects considered earlier [28].

### 2.1. In-medium vector meson masses

We now examine the medium modification to the masses of the  $\omega$ - and  $\rho$ -mesons in hot nuclear matter including the quantum correction effects in the relativistic random phase approximation. The interaction vertices for these mesons with nucleons are given as

$$\mathcal{L}_{\text{int}} = g_V \left( \bar{\psi} \gamma_\mu \tau^a \psi V_a^\mu - \frac{\kappa_V}{2M_N} \bar{\psi} \sigma_{\mu\nu} \tau^a \psi \partial^\nu V_a^\mu \right) \quad (2)$$

where  $V_a^\mu = \omega^\mu$  or  $\rho_a^\mu$ ,  $M_N$  is the free nucleon mass,  $\psi$  is the nucleon field and  $\tau_a = 1$  or  $\vec{\tau}$ ,  $\vec{\tau}$  being the Pauli matrices.  $g_V$  and  $\kappa_V$  correspond to the couplings due to the vector and tensor interactions for the corresponding vector mesons to the nucleon fields. The vector meson self energy is expressed in terms of the nucleon propagator,  $G(k)$  modified by the quantum effects. This is given as

$$\Pi^{\mu\nu}(k) = -\gamma_I g_V^2 \frac{i}{(2\pi)^4} \int d^4p \text{Tr} \left[ \Gamma_V^\mu(k) G(p) \Gamma_V^\nu(-k) G(p+k) \right], \quad (3)$$

where  $\gamma_I = 2$  is the isospin degeneracy factor for nuclear matter, and  $\Gamma_V^\mu(k) = \gamma^\mu \tau_a - \frac{\kappa_V}{2M_N} \sigma^{\mu\nu}$  represents the meson-nucleon vertex function. For the  $\omega$  meson, the tensor coupling, being small as compared to the vector coupling to the nucleons [6], is neglected [21, 22]. After carrying out the renormalization procedures for the vector self energies, the effective mass of the vector meson is obtained by solving the equation

$$k_0^2 - m_V^2 + \text{Re}\Pi(k_0, \mathbf{k} = 0) = 0. \quad (4)$$

where  $\Pi = \frac{1}{3}\Pi_\mu^\mu$ .

## 2.2. Meson decay properties

For a baryon-free environment,  $\rho \rightarrow \pi^+\pi^-$  is the dominant decay channel for  $\rho$  meson. The decay width for this process is calculated from the imaginary part of the self energy using the Cutkosky rule, and in the rest frame of the  $\rho$ -meson is given by

$$\Gamma_\rho(k_0) = \frac{g_{\rho\pi\pi}^2}{48\pi} \frac{(k_0^2 - 4m_\pi^2)^{3/2}}{k_0^2} \left[ \left(1 + f\left(\frac{k_0}{2}\right)\right) \left(1 + f\left(\frac{k_0}{2}\right)\right) - f\left(\frac{k_0}{2}\right)f\left(\frac{k_0}{2}\right) \right] \quad (5)$$

where,  $f(x) = [e^{\beta x} - 1]^{-1}$  is the Bose-Einstein distribution function. The first and the second terms in the equation (5) correspond to the decay and the formation of the resonance,  $\rho$ . In the calculation for the  $\rho$  decay width, the pion has been treated as free, and any modification of the pion propagator due to effects like delta-nucleon hole excitation [29] to yield a finite decay width for the pion, have not been taken into account. The coupling  $g_{\rho\pi\pi}$  is fixed from the decay width of  $\rho$  meson in vacuum ( $\Gamma_\rho=151$  MeV) decaying to two pions.

In the presence of baryons, however, it has been shown that there is considerable increase of the  $\rho$  decay width [17] in the thermal medium due to the scattering off the baryons. The dominant contributions which lead to appreciable broadening of the  $\rho$ - spectral function are the inelastic processes  $\rho N \rightarrow \pi N$  and  $\rho N \rightarrow \pi \Delta$ . The imaginary parts of the corresponding scattering amplitudes in the large baryon mass limit are given as [17]

$$\text{Im}T_{\rho N}^{(\pi N)} = g_A^2 \mathcal{H}(k_0, 0, m_\pi) \quad (6)$$

and

$$\text{Im}T_{\rho N}^{(\pi \Delta)} = 2g_A^2 \mathcal{H}(k_0, m_\Delta^* - m_N^*, m_\pi) \quad (7)$$

where,

$$\begin{aligned} \mathcal{H}(k_0, \Delta, m) = & \frac{g_{\rho NN}^2}{6\pi f_\pi^2} \left[ \frac{\sqrt{(k_0 - \Delta)^2 - m^2}}{(k_0^2 - 2k_0\Delta)^2} (3k_0^4 - 4k_0^2m^2 + 4m^4 + \Delta(8k_0m^2 - 12k_0^3)) \right. \\ & + \Delta^2(16k_0^2 - 8m^2) - 8\Delta^3k_0 + 4\Delta^4 \\ & \left. - \frac{\Delta(k_0^2 - 4m^2)^{3/2}}{2k_0(k_0^2 - 4\Delta^2)^2} (3k_0^2 - 8m^2 - 4\Delta^2) \right] \end{aligned} \quad (8)$$

In the above,  $g_A$  is the axial vector coupling constant chosen to be  $g_A = 1.26$  [17]. The  $\rho NN$  coupling is as fitted from the  $NN$  scattering data [30] and is given as  $g_{\rho NN}=2.6$ . We might note that, by definition, the  $\rho NN$  coupling used here is half of the coupling in Ref [17].

For high energies, the  $\rho N$  scattering process,  $\rho N \rightarrow \omega N$  also becomes important [17]. The corresponding scattering amplitude is given as

$$ImT_{\rho N}^{(\pi\omega)} = \frac{g_A^2 g_{\omega\rho\pi}^2}{48\pi f_\pi^2 m_\pi^2} \frac{k_0^2 k_\omega^2 \left[ 2k_\omega^2 m_N^{*2} - m_N^* (k_{\omega 0} - k_0) [(k_{\omega 0} - k_0)^2 - k_\omega^2] \right]}{m_N^* (m_N^* + k_0) (m_\pi^2 - m_\omega^{*2} + 2k_{\omega 0} k_0 - k_0^2)^2} \quad (9)$$

The interaction Lagrangian describing  $\omega\rho\pi$  as used above, is given as [32]

$$\mathcal{L}_{\omega\rho\pi} = \frac{g_{\omega\rho\pi}}{m_\pi} \epsilon_{\mu\nu\alpha\beta} \partial^\mu \omega^\nu \partial^\alpha \rho_i^\beta \pi_i \quad (10)$$

For the  $\omega\rho\pi$  coupling we take the value  $g_{\omega\rho\pi}=2$  according to Ref. [8] consistent with the decay width of  $\omega \rightarrow \pi\gamma$ . The  $\omega\rho\pi$  coupling as here is similar to that used in [33] after accounting for a factor of  $m_\pi/f_\pi$  difference in the definitions. In the above,  $|\vec{k}_\omega| = \sqrt{\lambda(m_N^* + k_0, m_\omega^*, m_N^*)}/(2(m_N^* + k_0))$  and  $k_{\omega 0} = \sqrt{m_\omega^{*2} + \vec{k}_\omega^2}$ . The Källén function  $\lambda$  is defined by  $\lambda(x, y, z) = (x^2 - (y + z)^2)(x^2 - (y - z)^2)$ . The present calculations for the collisional decay width of  $\rho$  meson take into account the mass modifications of the nucleon and vector mesons ( $\rho$  and  $\omega$ ). For  $\Delta$ , we assume that the mass scales in the same way as the nucleon mass in the medium, with  $m_\Delta=1232$  MeV as the mass in vacuum. It may be noted that the contributions given by (6), (7) and (9) to the  $\rho N$  scattering amplitude correspond to the zero temperature situation. The broadening of the  $\rho$  spectral function is significantly due to the finite density effects, which are expected to dominate over the temperature effects for the SPS conditions [23].

The contribution to the decay width of  $\rho$  due to  $\rho N$  scattering processes, arising from the  $\pi N$ ,  $\pi\Delta$  and  $\omega\pi$  loops are given in terms of the imaginary parts of the scattering amplitudes as [17]

$$\Gamma_{\rho N}^{coll} = \frac{\rho_B (ImT_{\rho N}^{(\pi N)} + ImT_{\rho N}^{(\pi\Delta)} + ImT_{\rho N}^{(\omega\pi)})}{k_0} \quad (11)$$

We might note here that the effect of  $\rho N$  scattering on the real part of the scattering amplitude has been seen to be negligible [17] and has not been considered here.

To calculate the decay width for the  $\omega$ -meson, we write down the effective Lagrangian for the  $\omega$  meson as [31, 32]

$$\mathcal{L}_\omega = -\frac{em_\omega^2}{g_\omega} \omega^\mu A_\mu + \frac{g_{\omega 3\pi}}{m_\pi^3} \epsilon_{\mu\nu\alpha\beta} \epsilon_{ijk} \omega^\mu \partial^\nu \pi^i \partial^\alpha \pi^j \partial^\beta \pi^k. \quad (12)$$

In the above, the first term refers to the direct coupling of the vector meson  $\omega$  to the photon, and hence to the dilepton pairs, as given by the vector dominance model. The decay width of the  $\omega$ -meson in vacuum is dominated by the channel  $\omega \rightarrow 3\pi$ . In the medium, the decay width for  $\omega \rightarrow 3\pi$  is given as

$$\Gamma_{\omega \rightarrow 3\pi} = \frac{(2\pi)^4}{2k_0} \int d^3\tilde{p}_1 d^3\tilde{p}_2 d^3\tilde{p}_3 \delta^{(4)}(P - p_1 - p_2 - p_3) |M_{fi}|^2 \left[ (1 + f(E_1))(1 + f(E_2))(1 + f(E_3)) - f(E_1)f(E_2)f(E_3) \right], \quad (13)$$

where  $d^3\tilde{p}_i = \frac{d^3p_i}{(2\pi)^3 2E_i}$ ,  $p_i$  and  $E_i$ 's are 4-momenta and energies for the pions, and  $f(E_i)$ 's are their thermal distributions. The matrix element  $M_{fi}$  has contributions from the channels

$\omega \rightarrow \rho\pi \rightarrow 3\pi$  (described by Eq. (10) and the direct decay  $\omega \rightarrow 3\pi$  resulting from the contact interaction (second term in (12)) [32, 33, 34]. After fitting  $g_{\omega\rho\pi}$  from the  $\omega \rightarrow \pi\gamma$  decay width, the point interaction coupling  $g_{\omega 3\pi}$  is determined by fitting the partial decay width  $\omega \rightarrow 3\pi$  in vacuum (7.49 MeV) to be 0.24 [22]. The contribution arising from the direct decay is up to around 15 %, which is comparable to the results of [32, 33].

With the modifications of the vector meson masses in the hot and dense medium, the contribution from the decay mode  $\omega \rightarrow \rho\pi$  becomes accessible [8, 22] when  $m_\omega^* > m_\rho^* + m_\pi$ . This is also considered in the present work. There may also be collisional broadening effects [17] for the  $\omega$  meson at high energies due to baryons. However, these are seen sensitive to the meson-baryon form factors [17] and have not been considered in the present calculations.

### 3. PARAMETRISATION OF THE PHOTON SELF ENERGY IN THE HADRONIC PHASE

Lattice simulations indicate that QCD undergoes a phase transition at a critical temperature,  $T_c$ , above which there is QGP phase, with quarks and gluons as the relevant degrees of freedom. As one approaches the critical temperature from the above, the quarks and gluons get confined to form the hadrons, which become the effective degrees of freedom for temperatures below  $T_c$ . In this section, we discuss the parametrisation of the photon self energy in the present scenario for the hadronic phase. The photon here couples to the vector mesons ( $\rho$  and  $\omega$ ) and the electromagnetic current-current correlator can be related to the currents generated by these mesons which are calculated using a Lagrangian describing the hadronic phase. The averaged photon spectral function is defined as [23]

$$R(q) = \frac{12\pi}{q^2} \text{Im}\bar{\Pi}(q), \quad (14)$$

where the photon self energy is related to the sum of the vector meson self energies as

$$\text{Im}\bar{\Pi}(q) = -\frac{1}{3} \sum_V \Pi_\mu^{\mu V}(q). \quad (15)$$

In the limit of  $\vec{q} \rightarrow 0$ , the averaged photon spectral function can be written as

$$R(q) = 12\pi q_0^2 \sum_V \text{Im}\Pi^V(q_0) \equiv 12\pi \sum_V \text{Im}\tilde{\Pi}^V(q_0). \quad (16)$$

In the Walecka model, the vector self energies can be parametrised as a Breit-Wigner distribution with an energy dependent decay width, along with a continuum as [35]

$$\text{Im}\tilde{\Pi}^V(q_0) = f_V^2 \frac{q_0 \Gamma_V(q_0)}{(q_0^2 - m_V^2)^2 + (q_0 \Gamma_V(q_0))^2} + \frac{C_V}{8\pi} \left(1 + \frac{\alpha_s(q_0)}{\pi}\right) \frac{1}{1 + e^{(q_0^V - q_0)/\delta}} \quad (17)$$

for the vector mesons,  $V = \rho, \omega$ . In the above,  $f_\rho$  and  $f_\omega$  are the coupling constants corresponding to the vector-meson-photon interactions. The continuum part is described as a smooth function in the energy [36, 37] instead of a step function as is usually adopted in QCD sumrule calculations [17, 38]. The values,  $C_\rho=1$  and  $C_\omega=1/9$  give the correct asymptotic limits for the spectral functions,  $\lim_{q_0 \rightarrow \infty} R_\rho = 3/2$  and  $\lim_{q_0 \rightarrow \infty} R_\omega = 1/6$  [17, 36, 37, 38]. Also, the energy dependence of the strong coupling constant occurring in the meson self energies has been taken into consideration and is given as  $\alpha_s(q_0) = 0.7/\ln(q_0/0.2)$  [36], where  $q_0$  is in units of GeV. The values for the parameters  $q_0^{\rho, \omega}$  correspond to the threshold energies above which asymptotic freedom is restored and quark model estimates for cross-sections become valid. The vacuum values for the parameters appearing in the continuum part of the spectral function as derived from the experimental data of  $e^+e^- \rightarrow \text{hadrons}$  are  $q_0^\rho = 1.3$  GeV,  $q_0^\omega = 1.1$  GeV, and  $\delta = 0.2$  GeV [36]. The vacuum values for the other parameters in the Breit-Wigner part of the photon spectral function are  $f_\rho=152$  MeV,  $f_\omega=50$  MeV,  $m_\rho=770$  MeV,  $m_\omega=783$  MeV,  $\Gamma_\rho=151$  MeV,  $\Gamma_\omega=7.5$  MeV. The masses of the vector mesons are replaced by the medium modified masses including quantum correction effects [22], as a simple pole approximation [38, 39]. However, the energy dependence of the decay widths is considered. We assume the medium modified threshold energies,  $q_0^{V*}$  to be given by the simple scaling [35]  $\frac{q_0^{V*}}{q_0} = \frac{m_V^*}{m_V}$ . The above parametrisation of the photon spectral function for the hadronic phase is used for studying the dynamical evolution of the strongly interacting matter arising in a ultrarelativistic heavy ion collision in an expanding fireball model [23]. In the following section, we briefly discuss the parametrisation of the photon self energy in the QGP phase described by a quasiparticle picture [19].

#### 4. PHOTON SELF ENERGY IN THE QGP PHASE

The QGP phase is described [19] using a quasiparticle picture. The model treats quarks and gluons as massive thermal quasiparticles with their properties determined so as to be compatible with the lattice QCD data. For temperatures much larger than  $T_c$ , the thermal masses can be calculated in the hard thermal loop (HTL) approximation using the perturbative QCD techniques. For temperatures near the phase transition, however, the coupling  $\alpha_s$  becomes large thus invalidating any perturbative techniques. Around  $T_c$ , a power law fall-off is assumed for the thermal masses, based on the conjecture that the phase transition is either weakly first order or second order as indicated by the lattice calculations. The thermodynamic quantities for the QGP are calculated in terms of two functions  $B(T)$  and  $C(T)$  introduced in the model, which account for the thermal vacuum energy and the onset of confinement for temperature approaching  $T_c$ . The quasiparticles are by construction

noninteracting and hence the quasiparticle  $q\bar{q}$  becomes the only contribution to the photon self energy [19]. In the QGP phase the time like photon couples to the continuum of thermally excited  $q\bar{q}$  states and subsequently converts into a dilepton pair, which gives the contribution to the dilepton emission rate from the QGP phase.

## 5. THE FIREBALL EVOLUTION MODEL

### 5.1. Expansion and flow

Our fundamental assumption is to treat the fireball matter as thermalized from an initial proper time scale  $\tau_0$  until breakup time  $\tau_f$ . For simplicity, we assume a spatially homogeneous distribution of matter. Since some volume elements move with relativistic velocities, it is sensible to choose volumes corresponding to a given proper time  $\tau$  for the calculation of thermodynamics, hence the thermodynamic parameters temperature  $T$ , entropy density  $s$ , pressure  $p$ , chemical potentials  $\mu_i$  and energy density  $\epsilon$  become functions of  $\tau$  only for such a system. In the following, we refer to  $\tau$  as the time measured in a frame co-moving with a given volume element.

In order to make use of the information coming from lattice QCD calculations, we proceed by calculating the thermodynamical response to a volume expansion that is parametrized in such a way as to reproduce the experimental information about the flow pattern and HBT correlations as closely as possible. As a further simplification, we assume the volume to be cylindrically symmetric around the beam (z)-axis. Thus, the volume is characterized by the longitudinal extension  $L(\tau)$  and the transverse radius  $R(\tau)$  and we find

$$V(\tau) = \pi L(\tau) R^2(\tau). \quad (18)$$

In order to account for collective flow effects, we boost individual volume elements according to a position-dependent velocity field. For the transverse flow, we make the ansatz

$$\eta_T(r, \tau) = r/R_{rms}(\tau) \eta_T^{rms}(\tau) \quad (19)$$

where  $R_{rms}(\tau)$  denotes the root mean square radius of the fireball at  $\tau$  and  $\eta_T^{rms}(\tau)$  the transverse rapidity at  $R_{rms}$ .

For the longitudinal dynamics, we start with the experimentally measured width of the rapidity interval of observed hadrons  $2\eta_f^{front}$  at breakup. From this, we compute the longitudinal velocity of the fireball front at kinetic freeze-out  $v_f^{front}$ . We do not require the initial expansion velocity  $v_0^{front}$  to coincide with  $v_f^{front}$  but instead allow for a longitudinally

accelerated expansion. This implies that during the evolution  $\eta = \eta_s$  is not valid (with  $\eta_s$  the spacetime rapidity  $\eta_s = 1/2 \ln((t+z)/(t-z))$ ) unlike in the non-accelerated case.

The requirement that the acceleration should be a function of  $\tau$  and that the system stays spatially homogeneous for all  $\tau$  determines the velocity field uniquely if the motion of the front is specified. We solve the resulting system of equations numerically [40]. We find that for not too large rapidities  $\eta < 4$  and accelerations volume elements approximately fall on curves  $const. = \sqrt{t^2 - z^2}$  and that the flow pattern can be approximated by a linear relationship between rapidity  $\eta$  and spacetime rapidity  $\eta_s$  as  $\eta(\eta_s) = \zeta \eta_s$  where  $\zeta = \eta^{front} / \eta_s^{front}$  and  $\eta_s^{front}$  is the rapidity of the cylinder front. In this case, the longitudinal extension can be found calculating the invariant volume  $V = \int d\sigma_\mu u^\mu$  as

$$L(\tau) \approx 2\tau \frac{\sinh((\zeta - 1)\eta_s^{front}(\tau))}{(\zeta - 1)} \quad (20)$$

with  $\eta_s^{front}(\tau)$  the spacetime rapidity of the cylinder front. This is an approximate generalization of the boost-invariant relation  $L(\tau) = 2\eta^{front}\tau$  which can be derived for non-accelerated motion.

## 5.2. Parameters of the expansion

In order to proceed, we have to specify the longitudinal acceleration  $a_z(\tau)$  (which in turn is used to calculate  $\eta_s^{front}(\tau)$  numerically), the initial front velocity  $v_0^{front}$  and the expansion pattern of the radius  $R(\tau)$  in proper time.

In principle, one would require  $a = \nabla p / \epsilon$ . However, our model framework contains a homogeneous distribution of matter, therefore  $\nabla p = 0$  everywhere except at the surface of the cylinder. In order to keep this approximation but nevertheless use a more realistic acceleration, we make the additional assumption that in a realistic situation a drop in temperature would leave the shape of the pressure distribution rather unchanged while reducing the overall magnitude. With this assumption,  $\nabla p \sim c \cdot p$ . Therefore, we make the ansatz

$$a_z = c_z \cdot \frac{p(\tau)}{\epsilon(\tau)} \quad (21)$$

which allows a soft point in the EoS where the ratio  $p/\epsilon$  gets small to influence the acceleration pattern.  $c_z$  and  $v_0^{front}$  are model parameters governing the longitudinal expansion and fit to data.

Since typically longitudinal expansion is characterized by larger velocities than transverse expansion, i.e.  $v_z^{front} \gg v_T^{front}$ , we treat the radial expansion non-relativistically. We assume

that the radius of the cylinder can be written as

$$R(\tau) = R_0 + c_T \int_{\tau_0}^{\tau} d\tau' \int_{\tau_0}^{\tau'} d\tau'' \frac{p(\tau'')}{\epsilon(\tau'')} \quad (22)$$

The initial radius  $R_0$  is taken from overlap calculations. This leaves a parameter  $c_T$  determining the strength of transverse acceleration which is also fit to data. The final parameter characterizing the expansion is its endpoint given by  $\tau_f$ , the breakup proper time of the system.

### 5.3. Thermodynamics

We assume that entropy is conserved throughout the thermalized expansion phase. Therefore, we start by fixing the entropy per baryon from the number of produced particles per unit rapidity (see e.g. [41]). Calculating the number of participant baryons (see [23]) we find the total entropy  $S_0$ . The entropy density at a given proper time is then determined by  $s = S_0/V(\tau)$ .

We describe the EoS in the partonic phase by a quasiparticle interpretation of lattice data which has been shown to reproduce lattice results both at vanishing baryochemical potential  $\mu_B$  and finite  $\mu_B$  [19] (see these references for details of the model).

For the phase transition temperature, we choose  $T_C = 170$  MeV based on lattice QCD computations at finite temperature for case of two light and one heavy quark flavour [42]. We also note that no large latent heat is observed in the transition and model the actual thermodynamics as a crossover rather than a sharp phase transition. Nevertheless, in the calculation we assume quarks and gluons as degrees of freedom above  $T_C$  and hadrons below to simplify computations. Since the time the system spends in the vicinity of the transition temperature is small compared with the total time for dilepton emission however, any error we make by this assumption is bound to be small as soon as we consider the measured rates which represent an integral over the time evolution of the system folded with the emission rate.

Since a computation of thermodynamic properties of a strongly interacting hadron gas close to  $T_C$  is a very difficult task, we follow a simplified approach in the following: We calculate thermodynamic properties of the hadron gas at kinetic decoupling where interactions cease to be important. Here, we have reason to expect that an ideal gas will be a good description and calculate the EoS with the help of an ideal resonance gas model. Using the framework of statistical hadronization [43], we determine the overpopulation of pion phase space by pions from decays of heavy resonances created at  $T_C$  and include this contribution (which gives rise to a pion-chemical potential of order  $\mu_\pi \approx 120$  MeV into the calculation.

We then choose a smooth interpolation between decoupling temperature  $T_f$  and transition temperature  $T_C$  to the EoS obtained in the quasiparticle description. This is described in greater detail in [23].

With the help of the EoS and  $s(\tau)$ , we are now in a position to compute the parameters  $p(\tau), \epsilon(\tau), T(\tau)$  as well. Since the ratio  $p(\tau)/\epsilon(\tau)$  appear in the expansion parametrization, we have to solve the model self-consistently.

#### 5.4. Solving the model

In order to adjust the model parameters, we compare with data on transverse momentum spectra and HBT correlation measurements. This is discussed in greater detail in [40, 44].

In [45], a very similar model is fit to a large set of experimental data, providing different sets of parameters  $T_f, v_{\perp f}, R_f, \eta_f^{front}$ . Although we use a different (box vs. Gaussian) longitudinal distribution of matter, we use the parameters from this analysis as a guideline for our transverse dynamics where this difference should not show up and determine  $\eta_f^{front}$  separately. Specifically, we use the set **b1** from [45] for the transverse dynamics.

By requiring  $R(\tau_f) = R_f$  and  $v_T^{front} = v_{\perp f}$  we can determine the model parameters  $c_T$  and  $\tau_f$ .  $c_z$  is fixed by the requirement  $\eta^{front}(\tau_f) = \eta_f^{front}$ . The remaining parameter  $v_0^{front}$  now determines the volume (and hence temperature) at freeze-out and can be adjusted such that  $T(\tau_f) = T_f$ .

The model for 5% central 158 AGeV Pb-Pb collisions at SPS is characterized by the following scales: Initial long. expansion velocity  $v_0^{front} = 0.5c$ , thermalization time  $\tau_0 = 1$  fm/c, initial temperature  $T_0 = 305$  MeV, duration of the QGP phase  $\tau_{QGP} = 7$  fm/c, duration of the hadronic phase  $\tau_{had} = 9$  fm/c, total lifetime  $\tau_f - \tau_0 = 16$  fm/c, r.m.s radius at freeze-out  $R_f^{rms} = 8.55$  fm, transverse expansion velocity  $v_{\perp f} = 0.537c$ .

For the discussion of dileptons, we require the fireball evolution for other than 5% central collisions. In this case, we make use of simple scaling arguments based on the initial overlap geometry and the number of collision participants. For a detailed description, see [23, 46].

In [23], it has been shown that this scenario is able to describe the measured spectrum of low mass dileptons, and in [43] it has been demonstrated that under the assumption of statistical hadronization at the phase transition temperature  $T_C$ , the measured multiplicities of hadron species can be reproduced. In [46], the model has been shown to describe charmonium suppression correctly. None of these quantities is, however, very sensitive to the detailed choice of the equilibration time  $\tau_0$ . Therefore, we have only considered the ‘canonical’ choice  $\tau_0 = 1$  fm/c so far. The calculation of photon emission within the present framework provides the opportunity to test this assumption and to limit the choice of  $\tau_0$ . In

[47], this has been investigated in some detail. Within the present framework, the limits  $0.5 \text{ fm/c} < \tau_0 < 3 \text{ fm/c}$  could be found. Variations within these limits, however, do not affect the spectrum of dileptons with invariant mass below 1 GeV significantly.

## 6. DILEPTON EMISSION

The emission of dileptons in the model is calculated using the differential emission rate

$$\frac{dN}{d^4x d^4q} = \frac{\alpha^2}{\pi^3 q^2} \frac{1}{e^{\beta q^0} - 1} \text{Im} \bar{\Pi}(q, T) = \frac{\alpha^2}{12\pi^4} \frac{R(q, T)}{e^{\beta q^0} - 1}, \quad (23)$$

where  $\alpha = e^2/4\pi$  and we have neglected the lepton masses. Eq.(23) is valid to order  $\alpha$  in the electromagnetic interaction and to all orders in the strong interaction. Its main ingredient is the temperature-dependent spectral function  $R(q, T)$ .

The differential rate of eq.(23) is integrated over the space-time history of the collision to compare the calculated dilepton rates with the CERES/NA45 data [1] taken in Pb-Au collisions at 158 AGeV (corresponding to a c.m. energy of  $\sqrt{s} \sim 17 \text{ AGeV}$ ) and 40 AGeV ( $\sqrt{s} \sim 8 \text{ AGeV}$ ). The CERES experiment is a fixed-target experiment. In the lab frame, the CERES detector covers the limited rapidity interval  $\eta = 2.1 - 2.65$ , *i.e.*  $\Delta\eta = 0.55$ . We integrate the calculated rates over the transverse momentum  $p_T$  and average over  $\eta$ , given that  $d^4p = M p_T dM d\eta dp_T d\theta$ . The formula for the space-time- and  $p$ -integrated dilepton rate hence becomes

$$\frac{d^2N}{dM d\eta} = \frac{2\pi M}{\Delta\eta} \int_{\tau_0}^{\tau_f} d\tau \int d\eta V(\eta, T(\tau)) \int_0^\infty dp_T p_T \frac{dN(T(\tau), M, \eta, p_T)}{d^4x d^4p} \text{Acc}(M, \eta, p_T), \quad (24)$$

where  $\tau_f$  is the freeze-out proper time of the collision,  $V(\eta, T(\tau))$  describes the proper time evolution of volume elements moving at different rapidities and the function  $\text{Acc}(M, \eta, p_T)$  accounts for the experimental acceptance cuts specific to the detector. At the CERES experiment, each electron/positron track is required to have a transverse momentum  $p_T > 0.2 \text{ GeV}$ , to fall into the rapidity interval  $2.1 < \eta < 2.65$  in the lab frame and to have a pair opening angle  $\Theta_{ee} > 35 \text{ mrad}$ . Finally, for comparison with the CERES data, the resulting rate is divided by  $dN_{ch}/d\eta$ , the rapidity density of charged particles.

As in [23], we also include the effects of the overpopulation of the pion phase space due to decay processes of heavy resonances to the emission from hadronic matter by introducing a temperature-dependent pion chemical potential  $\mu_\pi(T)$ .

In addition to the thermal emission of dileptons, we also consider dileptons from vacuum decays of vector mesons after the thermal decoupling of the fireball and hard dileptons from initial Drell-Yan processes. For details of the calculation of these contributions see ref. [23].

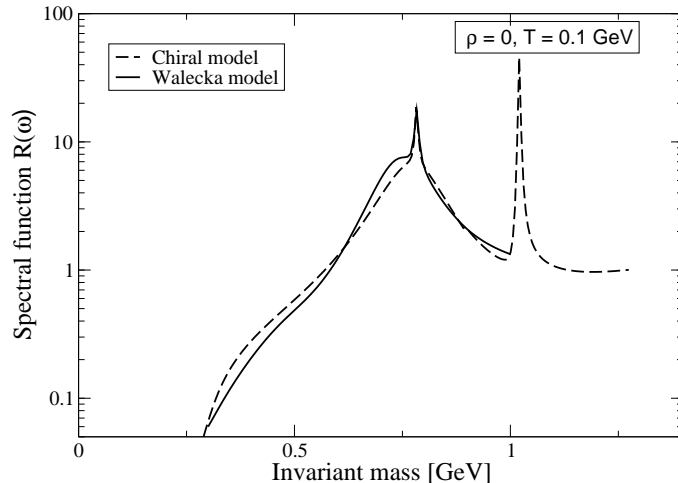


FIG. 1: Photon spectral function at  $T=100$  MeV.

A final remark: The spectral function considered in the present work is only available below 1 GeV invariant mass range. Therefore, we do not include thermal emission of dileptons from hadronic matter above that scale when discussing the Walecka model results. This leads to small differences between the two approaches for large invariant masses. This region, however, is not dominantly filled by emission from the hadronic phase but by the QGP and Drell-Yan contribution.

## 7. RESULTS AND DISCUSSIONS

We now discuss the results obtained for the photon spectral function in the hadronic matter arising due to medium modification of the vector mesons with the quantum correction effects from baryons and scalar mesons, and its effect on the dilepton emission spectra. Contrary to the mean field approximation, there is large drop of the vector meson masses due to vacuum polarisations from the nucleon sector. This shifts the  $\rho$  and  $\omega$  peaks in the dilepton spectra to lower values [22, 48]. The additional quantum correction effects from the sigma mesons lead to considerable increase of the  $\omega$  decay width [22].

In the present investigation, we choose the renormalised sigma meson self interaction coupling  $\lambda_R$  to be 5, corresponding to the value of incompressibility of nuclear matter to be 329 MeV [22]. As stated earlier, the dilepton spectra are studied in a mixed scenario of QGP and hadronic matter using the fireball model as described in the previous section. The photon spectral function as obtained in the present hadronic scenario is compared with

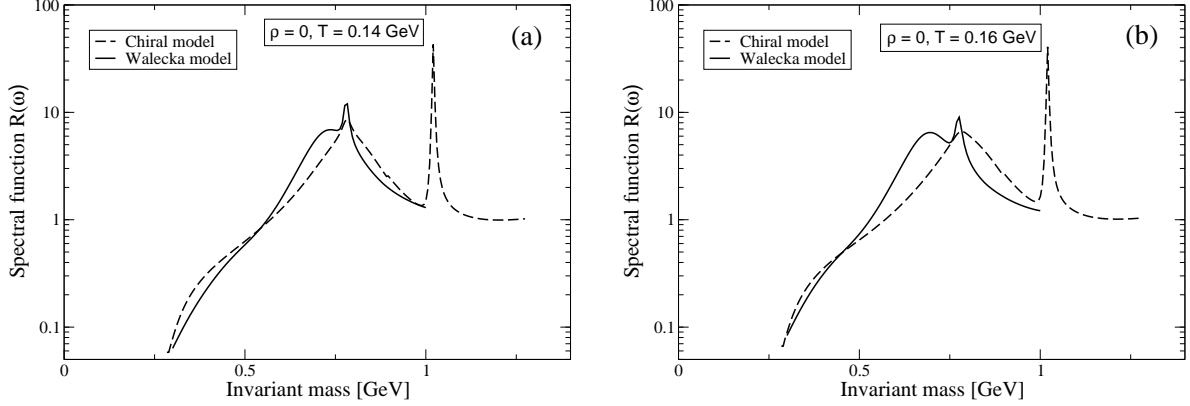


FIG. 2: Photon spectral function at  $T=140$  MeV and  $T=160$  MeV.

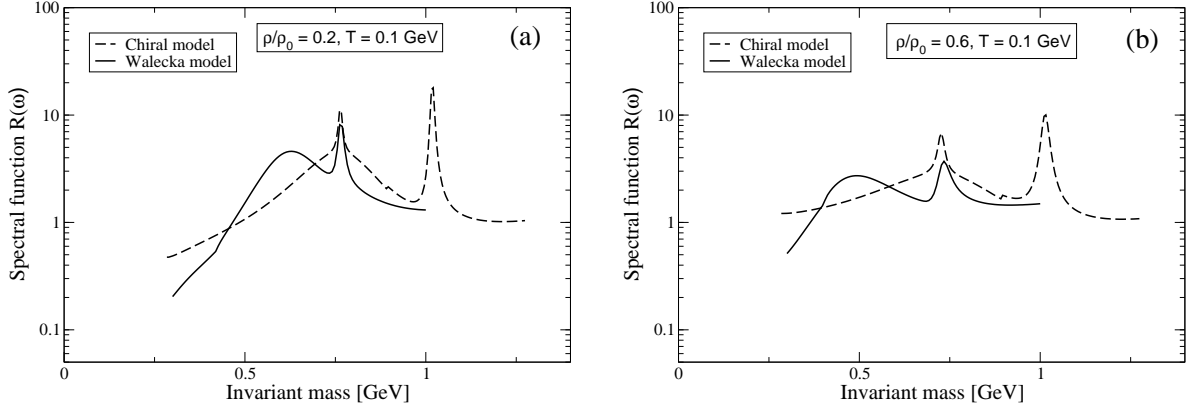


FIG. 3: Photon spectral function at  $T=100$  MeV and at densities  $0.2\rho_0$  and  $0.6\rho_0$ , with  $\rho_0=0.17$  fm $^{-3}$ .

the earlier calculation obtained in a chiral SU(3) model. This is described in [17] for finite density and [18] for finite temperature modifications. In [23], we assumed that it is possible to factorize these contributions.

The spectral functions in both the models are shown in figure 1 for vanishing baryon density and a temperature of 100 MeV. As expected due to absence of any pronounced medium effects for this temperature, the two models yield similar results.

In figure 2, the temperature dependence of the photon spectral function is shown. The spectral function in the present hadronic scenario is seen to develop a distinct  $\rho$  peak at higher temperatures. This is a reflection of the fact that with quantum correction effects,

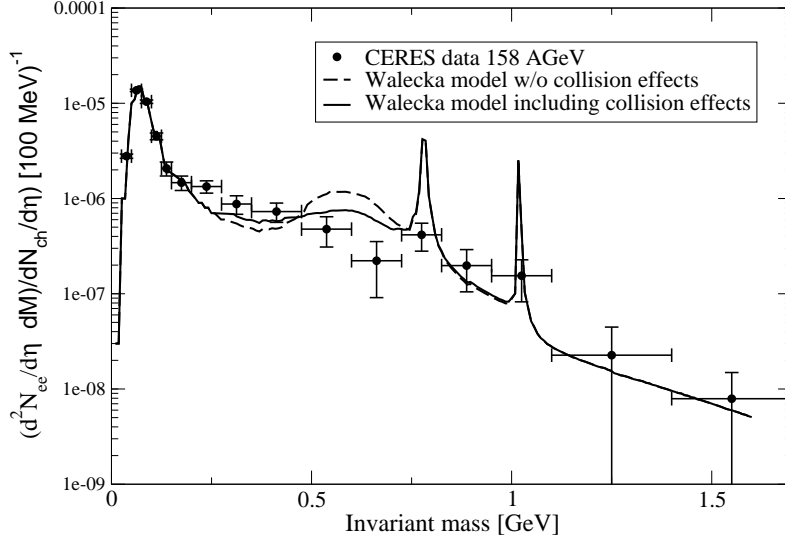


FIG. 4: Dilepton emission rate for 158 AGeV at SPS for the Walecka model with and without the collision effects.

the  $\rho$ -mass, due to the tensorial coupling, has a larger drop as compared to the mass of the  $\omega$ -meson. In the present calculations, the effect of temperature on the  $\rho$ -mass is rather moderate up to around a temperature of 160 MeV or so. This is in line with the previous calculation of [49]. The broadening of the  $\rho$  peak at higher temperature takes place as the Bose enhancement dominates over the effect of drop in  $\rho$ -mass, leading to an increase in the  $\rho$  decay width. On the other hand, the density dependence of the  $\rho$  mass is seen to be quite significant [22] which leads to the  $\rho$  peak position shifted to lower values in the present calculation as illustrated in figure 3. The mass of the  $\rho$ -meson remains almost unchanged in the chiral model, whereas the  $\rho$ -decay width has appreciable enhancement in the medium due to inelastic processes, like  $\rho N \rightarrow \pi N$ ,  $\rho N \rightarrow \pi \Delta$ , and also, from  $\rho N \rightarrow \omega N$  at higher energies. This basically leads to the  $\rho$  peak to be completely dissolved in the chiral model [17], leaving only a broad continuum. In the absence of collisional effects, the decay width for  $\rho$  arises from the process  $\rho \rightarrow \pi\pi$ . Here, the Bose-Einstein factors in (5) have the effect of increasing the width in the thermal medium, whereas the stronger dropping of the  $\rho$ -mass in the medium at higher densities in the present calculations has the opposite effect of decreasing the decay width and overcompensates the effect from the Bose enhancement factor. The collisional effects lead to considerable flattening of the spectral function for the  $\rho$  peak.

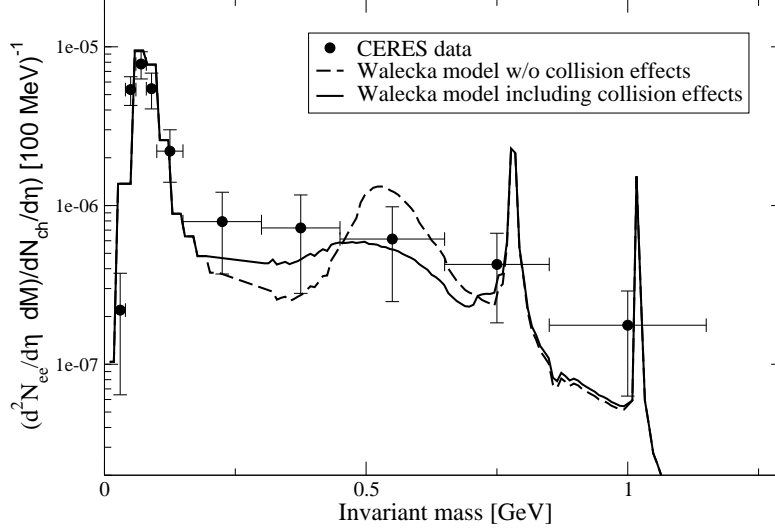


FIG. 5: Dilepton emission rate for 40 AGeV at SPS for the Walecka model with and without the collision effects.

Figures 4 and 5 show the dilepton spectra using the fireball model in the present hadronic scenario and a quasiparticle picture for QGP. The inclusion of collisional effects due to scattering off by the nucleons is seen to lead to considerable broadening of the  $\rho$ -peak in the dilepton spectra. The difference is seen to be more prominent for SPS 40 AGeV corresponding to a higher baryon density. The present hadronic scenario leads to a distinct structure in the dilepton emission rate due to the undissolved  $\rho$  peak in the absence of the contribution from the  $\rho N$  scattering processes, which is seen to be flattened due to these collision processes. The dropping of the vector meson masses in QHD in the relativistic Hartree approximation [48] also has been seen to yield similar results. In the absence of collisional processes, the drop in the  $\rho$  mass leads to enhancement in the dilepton yield below the vacuum  $\rho$  mass, but does not have the rather flat structure as observed in the data. Inclusion of inelastic processes  $\rho N \rightarrow \pi N$ ,  $\rho N \rightarrow \pi \Delta$ ,  $\rho N \rightarrow \omega N$ , give rise to considerable broadening of the spectra below the vacuum  $\rho$ -mass.

Figures 6 and 7 compare the dilepton emission rates of the present investigation to the results of chiral model description for hadronic matter as well as to the results from SPS, 158 AGeV and SPS, 40 AGeV 30% central Pb+Au collision. It may be noted that the fireball evolution, detector acceptance, contributions from the QGP and Drell-Yan background were modelled exactly in the same way for both theoretical curves. The previous hadronic scenario based on a chiral model [17, 18] has the observed dissolved  $\rho$  peak arising due to the

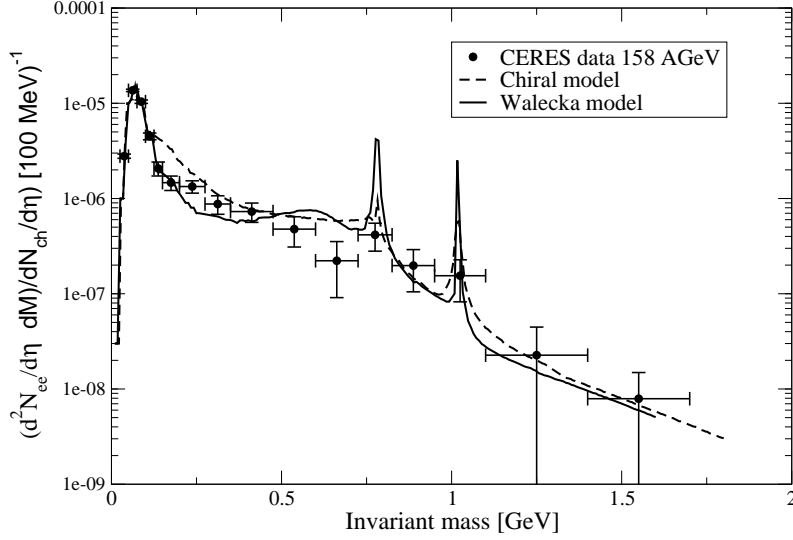


FIG. 6: Dilepton emission rate for 158 AGeV at SPS for the chiral and Walecka models.

Bose enhancement factors as well as the inelastic channels. In the present calculations, the collisions by nucleons lead to significant broadening of the  $\rho$ -peak in the dilepton spectra.

Contrary to what has been done in [23], we have not folded the results with the finite energy resolution of the detector in order to indicate what could be observed if the energy resolution were increased. The sharp peaks of  $\omega$  and  $\phi$  seen in the plots (absent in the plots in [23] and seemingly in contradiction with the data) represent vacuum decays of these mesons left after kinetic decoupling of the fireball. As apparent from [23], if the strength contained in these peaks is smeared out to represent finite detector resolution, agreement with the data is achieved.

In [50], dilepton and photon emission are studied using a more detailed description of the fireball matter using coarse-grained UrQMD and hydrodynamics. The essential scales of the expansion dynamics however appear similar to our approach - we also see dilepton emission for matter with average temperatures in the region between 120 and 250 MeV for a time period of about 15 fm/c. This is no surprise since essential scales of the evolution are dictated by the hadronic momentum spectra (and HBT radii) to which our model is adjusted. We might therefore expect that simplifying assumptions (such as introducing an average  $T$  for given  $\tau$ ) do not play a large role when one integrates over the complete four volume of the expansion.

It seems that the main difference which might account for the fact that our approach

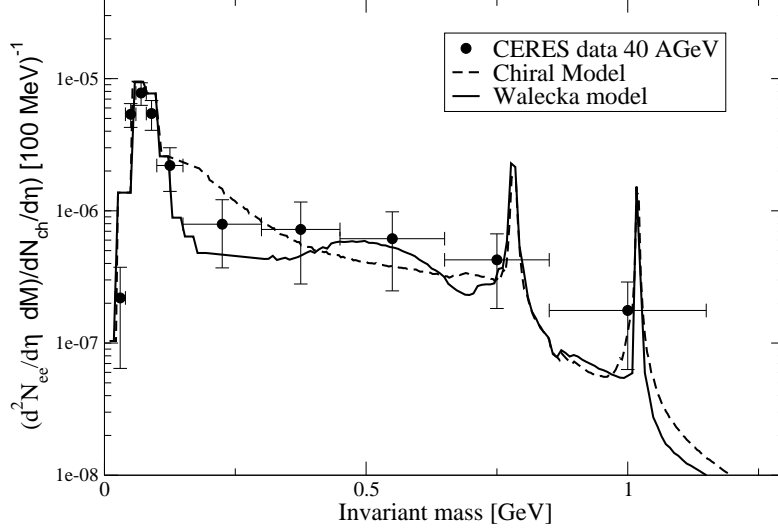


FIG. 7: Dilepton emission rate for 40 AGeV at SPS for the chiral and Walecka models.

describes the data well between 0.3 and 0.6 GeV invariant mass whereas [50] is somewhat on the low side is the use of different spectral functions. However, in order to test this a calculation in our framework using yet other spectral functions needs to be carried out which is beyond the scope of the present paper.

In [51], different approaches to describe the dilepton data for 158 AGeV beams are compared. Unfortunately, each of the calculations shown employs a different fireball model and a different description of in-medium modification of the vector mesons, emphasizing the need for studies along the line of the present paper. However, the emerging picture for BUU, transport and hydrodynamical calculations seems to be that to first approximation, the normalization of the dilepton invariant mass spectrum is determined by the fireball evolution, which is in turn strongly constrained by the hadronic momentum spectra and 2-particle correlations and should lead to similar essential scales of the fireball once the buildup of a pion chemical potential due to the decay of heavy resonances created at  $T_C$  is taken into account. The shape of the spectrum is then dictated by the spectral function. Here, a scenario employing a dropping in-medium  $\rho$  mass is shown to lead to similar results as broadening of the  $\rho$  peak due to the fact that a  $\rho$  mass dropping as a function of  $T$  sweeps through a large invariant mass region as  $T$  changes throughout the fireball evolution. In most approaches however, baryons seem to be crucial for the description of the spectral shape, in line with our own findings.

Unfortunately, the relations of the thermal fireball descriptions investigated in [51] to essential evolution scales is less clear — for example, no comment is made how transverse and longitudinal flow are implemented and what the relation of these models to the actual hadronic spectra at freeze-out would be and to what degree the models are tuned to reproduce dilepton data. Nevertheless, the resulting shape of the dilepton spectrum is expected to be close to a more detailed calculation whereas the normalization can be expected to be less certain.

Based on the present data, no clear distinction can be made between different approaches to calculate the photon spectral function at finite temperature and density. However, choosing a model which can be shown to describe other hadronic observables as well and using different spectral functions within one evolution model seems crucial to make progress in understanding the differences between the approaches on a more quantitative level.

## 8. SUMMARY

To summarize, we have investigated here the medium properties of the vector mesons in the Walecka model including the vacuum polarization effects and their effects on the dilepton spectra using a fireball model. The density dependence of the vector meson properties are seen to be the dominant medium effect as compared to the temperature dependence. We have considered a mixed scenario of QGP and hadronic matter [23] and have compared the dilepton emission rates of the present calculations to those from a previous calculation using a chiral SU(3) model, as well as to the experimental results from SPS at 158 AGeV and 40 AGeV.

Since the evolution of the fireball was not in any way adjusted to the dilepton data but rather fixed from different observables, we are in a position to compare the different spectral functions with the data without being subject to large uncertainties regarding the medium evolution.

Inclusion of vacuum polarisation effects in the Walecka model leads to dropping of these masses in the medium, contrary to the mean field approximation. This gives rise to the shift of the  $\rho$  and  $\omega$  peaks in the dilepton spectra to smaller values [22, 48]. Due to the stronger medium modification, the  $\rho$  peak is seen to be distinct from the  $\omega$  peak in the spectra. When the scattering due to nucleons is not taken into account in the present calculations, there is a more pronounced difference in the two models for SPS, 40 AGeV, as compared to SPS, 158 AGeV due to the higher baryon density. However, there is seen to be significant broadening of the spectra due to these collision effects within the present investigation.

## Acknowledgments

One of the authors (AM) would like to thank J. Reinhardt and S. Schramm for fruitful discussions. AM is grateful to the Institut für Theoretische Physik for warm hospitality and acknowledges financial support from Bundesministerium für Bildung und Forschung (BMBF). TR would like to thank W. Weise and R. A. Schneider for their support of this work. Financial support was given in part by BMBF and GSI.

- 
- [1] N. Masera for the HELIOS-3 collaboration, Nucl. Phys. **A 590**, 93c (1995); G. Agakichiev et al (CERES collaboration), Phys. Rev. Lett. **75**, 1272 (1995); G. Agakichiev et al (CERES collaboration), Phys. Lett. **B 422**, 405 (1998); G. Agakichiev et al (CERES collaboration), Nucl. Phys. **A 661**, 23c (1999); R. J. Porter et al (DLS collaboration), Phys. Rev. Lett. **79**, 1229 (1997); W. K. Wilson et al (DLS collaboration), Phys. Rev. C **57**, 1865 (1998).
  - [2] D. P. Morrison (PHENIX collaboration), Nucl. Phys. **A 638**, 565c (1998); J. Stroth (HADES collaboration), Advances Nuclear Dynamics **5**, 311 (1999).
  - [3] G. E. Brown and M. Rho, Phys. Rev. Lett. **66**, 2720 (1991).
  - [4] T. Hatsuda and Su H. Lee, Phys. Rev. **C 46**, R34 (1992); T. Hatsuda, S. H. Lee and H. Shiomi, Phys. Rev. **C 52**, 3364 (1995); X. Jin and D. B. Leinweber, Phys. Rev. **C 52**, 3344 (1995); T. D. Cohen, R. D. Furnstahl, D. K. Griegel and X. Jin, Prog. Part. Nucl. Phys. **35**, 221 (1995); R. Hofmann, Th. Gutsche, A. Faessler, Eur. Phys. J. **C 17**, 651 (2000); S. Mallik and K. Mukherjee, Phys. Rev. **D 58**, 096011 (1998); S. Mallik and A. Nyffeler, Phys. Rev. **C 63**, 065204 (2001); C. Ernst, S. A. Bass, M. Belkacem, H. Stöcker and W. Greiner, Phys. Rev. **C 58**, 447 (1998).
  - [5] H. Shiomi and T. Hatsuda, Phys. Lett. **B 334**, 281 (1994).
  - [6] T. Hatsuda, H. Shiomi and H. Kuwabara, Prog. Theor. Phys. **95**, 1009 (1996).
  - [7] H.-C. Jeans, J. Piekarewicz and A. G. Williams, Phys. Rev. **C 49**, 1981 (1994); K. Saito, K. Tsushima, A. W. Thomas, A. G. Williams, Phys. Lett. **B 433**, 243 (1998).
  - [8] Jan-e Alam, S. Sarkar, P. Roy, B. Dutta-Roy and B. Sinha, Phys. Rev. **C 59**, 905 (1999).
  - [9] R. Rapp and J. Wambach, Adv. Nucl. Phys. **25**, 1 (2000).
  - [10] W. Cassing and E. L. Bratkovskaya, Phys. Rep. **308**, 65 (1999).
  - [11] C. M. Ko, V. Koch and G. Q. Li, Ann. Rev. Nucl. Sci. **47**, 505 (1997).

- [12] Jan-e Alam, P. Roy, S. Sarkar and B. Sinha, nucl-th/0106038; Jan-e Alam, S. Sarkar, P. Roy, T. Hatsuda and B. Sinha, Ann. Phys. **286**, 159 (2000); F. Karsch, E. Laermann, P. Petreczky, S. Stickan, I. Wetzorke, hep-lat/0110208.
- [13] K. Redlich, J. Cleymans, V. V. Goloviznin, in Proceedings on NATO Advanced Workshop on Hot Hadronic Matter: Theory and Experiment, N.Y. Plenum Press, 1995, 562p; A. Dumitru, D. H. Rischke, Th. Schönfeld, L. Winkelmann, H. Stöcker and W. Greiner, Phys. Rev. Lett. **70**, 2860 (1993); P. Jaikumar, R. Rapp and I. Zahed, hep-ph/0112308; Song Gao, Ru-Keng Su, Xue- Qian Li, Comm. Theor. Phys. **28**, 207 (1997); D. Dutta, K. Kumar, A. K. Mohanty, R. K. Choudhury, Phys. Rev. **C 60**, 014905, 1999.
- [14] G. Q. Li, C. M. Ko and G. E. Brown, Phys. Rev. Lett **75**, 4007 (1995); G. Q. Li, C. M. Ko and G. E. Brown, Nucl. Phys. **A 606**, 568 (1996); G. Q. Li, C. M. Ko, G. E. Brown and H. Sorge, Nucl. Phys. **A 611**, 539 (1996).
- [15] E. L. Bratkovskaya and W. Cassing, Nucl. Phys. **A 619**, 413 (1997).
- [16] R. Rapp, G. Chanfray and J. Wambach, Phys. Rev. Lett. **76**, 368 (1996); R. Rapp, G. Chanfray and J. Wambach, Nucl. Phys. **A 661**, 472 (1997).
- [17] F. Klingl, N. Kaiser and W. Weise, Nucl. Phys. **A 624**, 527 (1997).
- [18] R. A. Schneider and W. Weise, Eur. Phys. J. A **9** (2000) 357; R. A. Schneider and W. Weise, Phys. Lett. B **515** (2001) 89.
- [19] R. A. Schneider and W. Weise, Phys. Rev. **C 64**, 055201 (2001); M. A. Thaler, R. A. Schneider and W. Weise, hep-ph/0310251.
- [20] A. Mishra, P. K. Panda, S. Schramm, J. Reinhardt and W. Greiner, Phys. Rev. **C 56**, 1380 (1997).
- [21] A. Mishra, J. C. Parikh and W. Greiner, Jour. Phys. **G 28**, 151 (2002).
- [22] A. Mishra, J. Reinhardt, H. Stoecker and W. Greiner, Phys. Rev. **C 66**, 064902 (2002).
- [23] T. Renk, R. A. Schneider and W. Weise, Phys. Rev. **C 66**, 014902 (2002); T. Renk, Ph.D. Thesis.
- [24] A. Mishra and H. Mishra, J. Phys. **G 23**, 143 (1997); S.Y. Pi and M. Samiullah, Phys. Rev. **D 36**, 3121 (1987); G. A. Camelia and S.Y. Pi, Phys. Rev. **D 47**, 2356 (1993); A. Mishra and H. Mishra, J. Phys. **G 23**, 143 (1997).
- [25] A. Mishra, P. K. Panda and W. Greiner, Jour. Phys. **G 27**, 1561 (2001).
- [26] A. Mishra, P. K. Panda and W. Greiner, Jour. Phys. **G 28**, 67 (2002).

- [27] H. Umezawa, H. Matsumoto and M. Tachiki, *Thermofield Dynamics and Condensed States* (North-Holland, Amsterdam, 1982).
- [28] B. D. Serot and J. D. Walecka, Adv. Nucl. Phys. **16**, 1 (1986); S. A. Chin, Ann. Phys. **108**, 301 (1977); S. Pal, Song Gao, H. Stöcker and W. Greiner, Phys. Lett. **B 465**, 282 (1999).
- [29] M. Asakawa, C. M. Ko, P. Levai and X. J. Qiu, Phys. Rev. **C 46**, R1159 (1992); M. Herrmann, B. L. Friman and W. Nörenberg, Nucl. Phys. **A 560**, 411 (1993); G. Chanfray and P. Shuck, Nucl. Phys. **A 545**, 271c (1992).
- [30] W. Grein, Nucl. Phys. **B 131**, 255 (1977); W. Grein and P. Kroll, Nucl. Phys. **A 338**, 332 (1980).
- [31] J. J. Sakurai, *Currents and Mesons* (The University of Chicago Press, Chicago, 1969); M. Gell-Mann, D. Sharp, and W. D. Wagner, Phys. Rev. Lett. **8**, 261 (1962).
- [32] B. A. Li, Phys. Rev. **D 52**, 5165 (1995).
- [33] F. Klingl, N. Kaiser and W. Weise, Z. Phys. **A 356**, 193 (1996).
- [34] Ö. Kaymakçalan, S. Rajeev and I. Schechter, Phys. Rev. **D 30**, 594 (1984).
- [35] J. Alam, S. Sarkar, P. Roy, T. Hatsuda, B. Sinha, Ann. Phys. **286**, 159, 2000.
- [36] E. V. Shuryak, Rev. Mod. Phys. **65**, 1 (1993).
- [37] J. I. Kapusta and E. V. Shuryak, Phys. Rev. **D 49**, 4694 (1994).
- [38] T. Hatsuda and S. H. Lee, Phys. Rev. **C 46**, R34 (1992).
- [39] J. Alam, S. Sarkar, P. Roy, B. Dutta-Roy, B. Sinha, Phys. Rev. **C 59**, 905 (1999).
- [40] T. Renk, hep-ph/0403239.
- [41] J. Letessier, A. Tounsi, U. Heinz, J. Sollfrank and J. Rafelski, Phys. Rev. **D51** (1995) 3408.
- [42] F. Karsch, E. Laermann and A. Peikert, Nucl. Phys. **B 605** (2001) 579.
- [43] T. Renk, hep-ph/0210307.
- [44] T. Renk, hep-ph/0310346.
- [45] B. Tomasik, U. A. Wiedemann and U. W. Heinz, nucl-th/9907096.
- [46] A. Polleri, T. Renk, R. Schneider and W. Weise, nucl-th/0306025.
- [47] T. Renk, Phys. Rev. **C 67** (2003) 064901.
- [48] S. Sarkar, Jan-e Alam and T. Hatsuda, nucl-th/0011032.
- [49] C. Gale and J. I. Kapusta, Nucl. Phys. **B 357**, 65 (1991).
- [50] P. Huovinen, M. Belkacem, P. J. Ellis and J. I. Kapusta, Phys. Rev. **C 66** (2002) 014903.
- [51] R. Rapp and J. Wambach, Adv. Nucl. Phys. **25** (2000) 1.